Atmos. Chem. Phys., 11, 4209–4219, 2011
www.atmos-chem-phys.net/11/4209/2011/
doi:10.5194/acp-11-4209-2011

Atmospheric Chemistry and Physics

Global and regional effects of the photochemistry of $CH_3O_2NO_2$: evidence from ARCTAS

E. C. Browne[1], A. E. Perring[1,*,], P. J. Wooldridge[1], E. Apel[2], S. R. Hall[2], L. G. Huey[3], J. Mao[4], K. M. Spencer[5], J. M. St. Clair[6], A. J. Weinheimer[2], A. Wisthaler[7], and R. C. Cohen[1,8]**

[1]Department of Chemistry, University of California Berkeley, Berkeley, CA, USA
[2]Atmospheric Chemistry Division, National Center for Atmospheric Research, Boulder, CO, USA
[3]School of Earth and Atmospheric Sciences, Georgia Institute of Technology, Atlanta, GA, USA
[4]School of Engineering and Applied Science, Harvard University, Cambridge, MA, USA
[5]Division of Chemistry and Chemical Engineering, California Institute of Technology, Pasadena, CA, USA
[6]Division of Geology and Planetary Sciences, California Institute of Technology, Pasadena, CA, USA
[7]Institut für Ionenphysik & Angewandte Physik, University of Innsbruck, Innsbruck, Austria
[8]Department of Earth and Planetary Sciences, University of California Berkeley, Berkeley, CA, USA
[*]now at: Chemical Sciences Division, Earth Systems Research Laboratory, National Oceanic and Atmospheric Administration, Boulder, CO, USA
[**]now at: Cooperative Institute for Research in Environmental Sciences, University of Colorado, Boulder, CO, USA

Received: 20 December 2010 – Published in Atmos. Chem. Phys. Discuss.: 21 January 2011
Revised: 27 April 2011 – Accepted: 28 April 2011 – Published: 6 May 2011

Abstract. Using measurements from the NASA Arctic Research of the Composition of the Troposphere from Aircraft and Satellites (ARCTAS) experiment, we show that methyl peroxy nitrate ($CH_3O_2NO_2$) is present in concentrations of ∼5–15 pptv in the springtime arctic upper troposphere. We investigate the regional and global effects of $CH_3O_2NO_2$ by including its chemistry in the GEOS-Chem 3-D global chemical transport model. We find that at temperatures below 240 K inclusion of $CH_3O_2NO_2$ chemistry results in decreases of up to ∼20 % in NO_x, ∼20 % in N_2O_5, ∼5 % in HNO_3, ∼2 % in ozone, and increases in methyl hydrogen peroxide of up to ∼14 %. Larger changes are observed in biomass burning plumes lofted to high altitude. Additionally, by sequestering NO_x at low temperatures, $CH_3O_2NO_2$ decreases the cycling of HO_2 to OH, resulting in a larger upper tropospheric HO_2 to OH ratio. These results may impact some estimates of lightning NO_x sources as well as help explain differences between models and measurements of upper tropospheric composition.

1 Introduction

Non-acyl peroxynitrates (e.g. HO_2NO_2, $CH_3O_2NO_2$) are weakly bound molecules that play a role in the chemistry of the troposphere where it is cold (Slusher et al., 2002; Murphy et al., 2004; Kim et al., 2007) or where peroxy radicals and NO_x ($NO_x = NO + NO_2$) have especially high concentrations (Spencer et al., 2009). Initial observations and calculations focused on understanding the role these molecules play in the stratospheric HO_x ($HO_x = OH + HO_2$) balance (e.g. Wennberg et al., 1999). More recently, in-situ observations of non-acyl peroxynitrates in the troposphere (Slusher et al., 2002; Murphy et al., 2004; Kim et al., 2007; Spencer et al., 2009) have resulted in increased interest in the role of these compounds in NO_x and HO_x budgets in the lower troposphere. During the NCAR Tropospheric Ozone Production about the Spring Equinox (TOPSE) experiment (Atlas et al., 2003), measurements in the Arctic upper troposphere, where temperatures were on average ∼230 K, showed that non-acyl peroxy nitrates, primarily HO_2NO_2, were on average, 30 % of NO_y ($NO_y = NO + NO_2 + HO_2NO_2 + CH_3O_2NO_2 + HNO_3 + HONO$ + acyl peroxy nitrates + organic nitrates + NO_3 + $2\,N_2O_5$) (Murphy et al., 2004). These observations imply that HO_2NO_2 represents a significant sink of HO_x and acts as a large reservoir of NO_x in the Arctic during winter and spring. Measurements from

---

Correspondence to: R. C. Cohen
(rccohen@berkeley.edu)

Table 1. Measurements used in this analysis to constrain the photostationary state model. XNO_2 refers to the sum of NO_2 and the fraction of $CH_3O_2NO_2 + HO_2NO_2$ that thermally dissociate in the inlet of the LIF instrument.

Species	Method	Reference
NO, O_3	Chemiluminescence	Weinheimer et al. (1994)
XNO_2	LIF[a]	Thornton et al. (2000); Cleary et al. (2002)
Pernitric acid, peracetic acid, methyl hydrogen peroxide	CIMS[b]	Crounse et al. (2006, 2009) St. Clair et al. (2010)
Acetone	PTR-MS[c]	Wisthaler et al. (2002)
Acetaldehyde	GC-MS[d]	Apel et al. (2003)
Peroxyacetyl nitrate	CIMS[b]	Slusher et al. (2004); Kim et al. (2007)
CH_4	TDLAS[e]	Sachse et al. (1987); Diskin et al. (2002)
OH, HO_2	LIF[a] CIMS[b]	Faloona et al. (2004); Cantrell et al. (2003a)
UV photolytic frequencies	Spectral radiometry	Shetter and Müller (1999)

[a] Laser Induced Fluorescence [b] Chemical ionization mass spectrometry [c] Proton transfer reaction mass spectrometry [d] Gas chromatography – mass spectrometry
[e] Tunable diode laser absorption spectroscopy

the NASA Intercontinental Chemical Transport Experiment-North America (INTEX-NA) demonstrated that HO_2NO_2 is present in the mid-latitude upper troposphere at mixing ratios of approximately 76 pptv between 8 and 9 km, accounting for about 5 % of NO_y and 10 % of the local HO_x sink (Kim et al., 2007).

HO_2NO_2 is formed by the association reaction of HO_2 and NO_2 and methyl peroxy nitrate ($CH_3O_2NO_2$) is formed by the analogous association reaction of CH_3O_2 with NO_2. Although CH_3O_2 is the second most abundant peroxy radical in the atmosphere (after HO_2), much less attention has been devoted to $CH_3O_2NO_2$ chemistry. To our knowledge the indirect measurement of the sum of HO_2NO_2 and $CH_3O_2NO_2$ during the TOPSE campaign by Murphy et al. (2004) is the only previous in-situ evidence for $CH_3O_2NO_2$. $CH_3O_2NO_2$ chemistry has been previously considered in some box and one dimensional models. Thompson et al. (1997) used a 1-D tropospheric chemical model and upper tropospheric measurements from the Pacific Exploratory Mission in the Western Pacific Ocean (PEM-West B) and predicted a mean concentration of 27 pptv for $CH_3O_2NO_2$ at 10 km in the mid-latitudes (35°–45° N) during February and March. During TOPSE, a steady-state model indicated that at temperatures around 250 K $CH_3O_2NO_2$ should be present at average concentrations of 70 pptv (at 40°–60° N) and 27 pptv (at 60°–85° N) (Cantrell et al., 2003b). Here we present experimental evidence from observations during the Arctic Research of the Composition of the Troposphere from Aircraft and Satellites (ARCTAS) experiment for the presence of $CH_3O_2NO_2$. We use the GEOS-Chem (Bey et al., 2001) 3-D chemical transport model to investigate the effects of $CH_3O_2NO_2$ chemistry on the distribution of NO_x, O_3, NO_y, and HO_y ($HO_y = OH + HO_2 + HONO + HO_2NO_2 + CH_3OOH + 2\,H_2O_2$) species. We find that at temperatures below 240 K, the addition of $CH_3O_2NO_2$ chemistry to GEOS-Chem decreases regional concentrations of NO_x by 20 % and of O_3 by 2 %. Additionally, concentrations of N_2O_5 decrease by ∼20 % and methyl hydrogen peroxide concentrations increase by ∼14 %.

2 Measurements

The ARCTAS measurement campaign has been described in detail by Jacob et al. (2010). Here we focus on the spring portion of ARCTAS (ARCTAS-A) which took place 1–19 April 2008. ARCTAS-A consisted of two transit flights between Palmdale, CA and Fairbanks, Alaska (65° N, 148° W) and seven arctic flights. The arctic flights included three local flights as well as flights to and from Thule, Greenland (77° N, 69° W) and Iqaluit, Nunavut (64° N, 69° W). In this analysis we only consider data collected north of 55° N.

The payload of the DC-8 consisted of an extensive suite of gas phase and aerosol measurements (Jacob et al., 2010). In our analysis we use the measurements listed in Table 1. All data are available in a public archive (http://www-air.larc.nasa.gov/cgi-bin/arcstat-c). Although OH and HO_2 were measured both by the NCAR chemical ionization mass spectrometer (Cantrell et al., 2003a) and the Pennsylvania State laser induced fluorescence (LIF) techniques (Faloona et al., 2004), we use the LIF OH and HO_2 measurements in our model due to the more extensive coverage at high altitudes.

The core measurements for this analysis are from the UC Berkeley nitrogen oxides instrument. Briefly, total peroxy nitrates (Σ PNs), total alkyl and multifunctional nitrates (Σ ANs), and NO_2 were measured using the Thermal Dissociation-Laser Induced Fluorescence (TD-LIF) instrument described in detail by Wooldridge et al. (2010). NO_2 is measured using laser induced fluorescence (Thornton et al., 2000) with supersonic expansion (Cleary et al., 2002). A 7 kHz, Q-switched, frequency doubled Nd:YAG laser pumps a tunable dye laser utilizing a mixture of pyrromethene 597 in isopropanol. This produces narrowband radiation

($0.06\,cm^{-1}$) at 585 nm. The laser light is focused through two multipass white cells and the red-shifted fluorescence (wavelengths long of 700 nm) is detected using a red sensitive photomultiplier tube (Hamamatsu H7421-50). Prompt scatter is eliminated using time gated detection and scattered light with wavelengths less than 700 nm is rejected by bandpass filters. Fluorescence counts are collected at 4 Hz and averaged to one second for reporting to the data archive. We tune the dye laser on and off an isolated rovibronic feature of the jet-cooled NO_2 at 585 nm. The frequency is held at the peak of the feature for 9 s and then moved to the offline position in the continuum absorption of NO_2 for 3 s. The difference between these two signals is directly proportional to the NO_2 mixing ratio. The ratio between the peak and background NO_2 fluorescence is 10 to 1 at 760 torr backing pressure behind the expansion nozzle. The detection cells are kept at a pressure of approximately 0.2 torr. Calibration is performed at least every two hours during a level flight leg using a 4.5 ppm NO_2 reference standard diluted to ∼2–8 ppbv in zero air. Stability of the NO_2 reference is verified by comparing a library of 6–8 different NO_2 standards approximately twice a year. These standards have been observed to remain stable for up to 5 years and to be accurate at atmospherically relevant mixing ratios to within 1 % (Bertram et al., 2005). As described in Thornton et al. (2000), correction for fluorescence quenching by water is made using the DLH measurements (Sachse et al., 1987; Diskin et al., 2002).

The configuration of the instrument for ARCTAS consisted of two detection cells. Sample flow was directed through a short (18 cm) inlet heated to approximately 25 °C and then split into two sampling lines. Two-thirds of the flow is directed down 154.5 cm of PFA tubing at cabin temperature before splitting in two. Half of this flow is directed to detection cell 1 for ambient NO_2 measurement. The other half is heated in a quartz tube at 200 °C to thermally dissociate peroxy nitrates and then passes through PFA tubing to detection cell 2. The remaining third of the sample flow is passed directly into a heated quartz tube (375 °C) followed by PFA tubing for Σ ANs detection in detection cell 2. NO_2 was measured continuously in cell 1 while cell 2 alternately sampled the $NO_2 + \Sigma$ PNs signal (50 % of the time) and the $NO_2 + \Sigma$ PNs $+ \Sigma$ ANs signal (50 % of the time).

During ARCTAS, NO_2 was also measured by photolytic conversion to NO with detection via chemiluminescence from the reaction of NO and ozone (Weinheimer et al., 1994). For the one minute merged data (version 11) the measurements agree within the stated uncertainties. A linear least-squares non-weighted fit (as in Cantrell, 2008) of the chemiluminescence data versus the LIF data resulted in a slope of 0.95 ± 0.01 with an intercept of -8.1 ± 0.8 pptv and an R^2 value of 0.95.

3 Observational evidence of $CH_3O_2NO_2$

Methyl peroxy nitrate is weakly bound (∼95 $kJ\,mol^{-1}$) and calculations (performed after ARCTAS was completed) suggest that it dissociates with high efficiency in the inlet lines of the TD-LIF instrument after which it is detected in the NO_2 channel. The interference from $CH_3O_2NO_2$ is expected to affect both the LIF and chemiluminescence NO_2 measurements. It is likely that past measurements of NO_2 in the upper troposphere and arctic are subject to this interference from $CH_3O_2NO_2$. This may explain discrepancies between observed and modeled upper tropospheric NO_2 in past experiments (e.g. Crawford et al., 1996). Additionally, it is consistent with the improvement between upper tropospheric measured and modeled NO_2 observed by Bradshaw et al. (1999) between the 1991 PEM-West-A experiment and 1996 PEM-Tropics-A experiment when the inlet was redesigned to decrease the residence time to 40 ms (from 2 s). Here we focus on $CH_3O_2NO_2$ and its behavior in the LIF instrument as it was configured during ARCTAS. In what follows we refer to this measurement as XNO_2 to indicate that it is a measurement of the sum of NO_2 and a fraction of these thermally labile nitrogen compounds.

Given a 300 K cabin temperature (approximate mean cabin temperature during ARCTAS) and a pressure of 300 torr, the thermal decomposition lifetime of $CH_3O_2NO_2$ is 700 ms, while that of HO_2NO_2 is 17.9 s. Although the residence time of an ambient sample in our detection system is quite short (∼350–850 ms), we calculate that between 48 and 77 % of $CH_3O_2NO_2$ and 3 to 6 % of HO_2NO_2 thermally dissociate prior to reaching the NO_2 detection cell. HO_2NO_2 dissociation is minimal and results in a median calculated NO_2 interference of less than 1 ppt (6 % of the XNO_2 signal) and a maximum absolute interference during a 1 minute period of 10.3 ppt (19 % of the NO_2 signal). This molecule is detected with near unit efficiency in the Σ PNs channel as described previously (Murphy et al., 2004; Wooldridge et al., 2010).

We calculate the ambient $CH_3O_2NO_2$ concentration using an instantaneous photostationary state model subject to the constraint that the sum of the model NO_2 and the fractions of HO_2NO_2 and $CH_3O_2NO_2$ that dissociate in the LIF inlet are equal to the LIF measurement of XNO_2. We used measured concentrations of HO_2NO_2 to calculate the contribution of HO_2NO_2 to the XNO_2 measurement. Since the validity of the photostationary state assumption requires that the source and sink reactions of a molecule vary slowly in comparison to the lifetime of that molecule, we perform this calculation only when the lifetime of $CH_3O_2NO_2$ is less than 12 h, or there is greater than 20 h of sunlight per day as in Murphy et al. (2004). Additionally, we filter the data to exclude locations where tropospheric composition has been recently perturbed. These include times when the DC-8 sampled fresh NO_x emissions (defined as $NO_x/NO_y > 0.2$ and when NO was more than ±3 standard deviations of the median value within ±0.5 km altitude), ozone

Table 2. Reactions and rates used in the photostationary state model.

	Reaction	Rate Constant
1	$CH_4 + OH + O_2 \rightarrow CH_3O_2 + H_2O$	$2.45\times10^{-12}\times\exp(-1775/T)^a$
2	$CH_3C(O)O_2 + NO \rightarrow CH_3O_2 + CO_2 + NO_2$	$8.1\times10^{-12}\times\exp(270/T)^a$
3	$CH_3C(O)CH_3 + h\nu + 2\,O_2 \rightarrow CH_3C(O)O_2 + CH_3O_2$	Measured
4	$CH_3C(O)O_2 + CH_3C(O)O_2 + 2\,O_2 \rightarrow 2\,CH_3O_2 + 2\,CO_2 + O_2$	$2.9\times10^{-12}\times\exp(500/T)^a$
5	$CH_3OOH + OH \xrightarrow{70\%} CH_3O_2 + H_2O$	$3.8\times10^{-12}\times\exp(200/T)^a$
6	$CH_3C(O)H + h\nu + O_2 \rightarrow CH_3O_2 + HCO$	Measured
7	$CH_3O_2NO_2 + h\nu \rightarrow CH_3O_2 + NO_2$	Assumed to be equal to measured HO_2NO_2 value
8	$CH_3O_2NO_2 + h\nu \rightarrow CH_3O + NO_3$	Assumed to be equal to measured HO_2NO_2 value
9	$CH_3O_2 + NO \rightarrow CH_3O + NO_2$	$2.8\times10^{-12}\times\exp(300/T)^a$
10	$CH_3O_2 + HO_2 \rightarrow$ Products	$3.8\times10^{-13}\times\exp(780/T)^b$
11	$CH_3O_2 + CH_3C(O)O_2 \rightarrow$ Products	$2.0\times10^{-12}\times\exp(500/T)^a$
12	$CH_3O_2 + CH_3O_2 \rightarrow$ Products	$9.5\times10^{-14}\times\exp(390/T)^a$
13	$CH_3O_2 + NO_2 + M \leftrightarrow CH_3O_2NO_2 + M$	Low Pressure Limit = $1.0\times10^{-30}\times(T/300)^{-4.8}$ High Pressure Limit = $7.2\times10^{-12}\times(T/300)^{-2.1}$ $K_{eq} = 9.5\times10^{-29}\times\exp(11234/T)^a$
14	$CH_3C(O)O_2NO_2 + h\nu \rightarrow CH_3C(O)O_2 + NO_2$	Measured
15	$CH_3C(O)O_2NO_2 \leftrightarrow CH_3C(O)O_2 + NO_2$	Low Pressure Limit = $9.7\times10^{-29}\times(T/300)^{-5.6}$ High Pressure Limit = $9.3\times10^{-12}\times(T/300)^{-1.5}$ $K_{eq} = 9.0\times10^{-29}\times\exp(14\,000/T)^a$
16	$CH_3C(O)OOH + OH \rightarrow CH_3C(O)O_2 + H_2O$	$3.7\times10^{-12\,c}$
17	$CH_3C(O)H + OH + O_2 \rightarrow CH_3C(O)O_2 + H_2O$	$4.7\times10^{-12}\times\exp(345/T)^b$
18	$CH_3C(O)O_2 + HO_2 \rightarrow$ Products	$5.2\times10^{-13}\times\exp(980/T)^b$

[a] JPL 2006 (Sander et al., 2006); [b] Atkinson et al. (2006) (web version last updated 2009 http://www.iupac-kinetic.ch.cam.ac.uk/show_datasheets.php?category=gas-phase+organics%3a+hox+%2b+voc+%28c1-c3%29); [c] Master Chemical Mechanism v3.1 (Saunders et al., 2003)

depletion events ($O_3 < 20$ ppb), stratospheric influences (defined as $O_3/CO > 0.75$), and solar zenith angle greater than 85 degrees. These restrictions exclude measurements from the coldest temperatures/highest altitudes sampled during ARCTAS: conditions under which we would expect high concentrations of $CH_3O_2NO_2$.

The reactions included in the photostationary state calculation are shown in Table 2. All measured values are from the archived one minute merged data, version 11. In addition to the XNO_2 measurement, concentrations of species listed in Table 1 were used to constrain the model. The use of the measured OH and HO_2 concentrations enables us to exclude HO_x source reactions from our photostationary state model. As the IUPAC recommended UV cross sections for $CH_3O_2NO_2$ (Atkinson et al., 2006) are identical to HO_2NO_2 (Atkinson et al., 2004), we set the UV photolysis of $CH_3O_2NO_2$ equal to the measured UV photolysis rate of HO_2NO_2. We do not consider infrared overtone photolysis of $CH_3O_2NO_2$ due to the shorter thermal decomposition lifetime of $CH_3O_2NO_2$ and the lower expected cross section of C-H overtones (Nizkorodov et al., 2005; Vaida, 2009). The model is run to steady state concentrations (±0.001 %) for peroxyacetyl radical, methyl peroxy radical, and $CH_3O_2NO_2$. We do not attempt to fill in missing data points from any of the measured species and calculate concentrations for the 480 one minute averaged data points which meet our selection criteria.

Uncertainties in our model calculations of NO_2 and $CH_3O_2NO_2$ will be a combination of systematic and random uncertainties in the measured concentrations and systematic uncertainties in the photolysis rates, the rate constants, and the estimated residence time in our instrument prior to detection. Uncertainties in the rate constants for $CH_3O_2NO_2$ formation and dissociation and in the instrument residence time will have the largest systematic effect on our results. In our calculation we use the JPL-2006 (Sander et al., 2006) rate recommendations for $CH_3O_2NO_2$ reactions. This recommendation is based on the recent work of Golden (2005), who has re-evaluated the data for formation and dissociation of $CH_3O_2NO_2$. This re-evaluation includes the new measurements of the association reaction of CH_3O_2 and NO_2 by Bacak et al. (2006). The measurement of Bacak et al. (2006) at 223 K represents the first measurements of the rate constant below 253 K, thus significantly reducing the uncertainty in this reaction at low temperatures. Adjusting the uncertainties to the JPL-2006 one sigma values for the rate constants of formation and decomposition of $CH_3O_2NO_2$ results in changes to the calculated NO_2 values of $\sim\pm23\,\%$ ($\sim$1.2 ppt) and of $\mp40\,\%$ ($\sim$2.3 ppt) for $CH_3O_2NO_2$ in the temperature range of 230–235 K. This range of NO_2 concentrations is

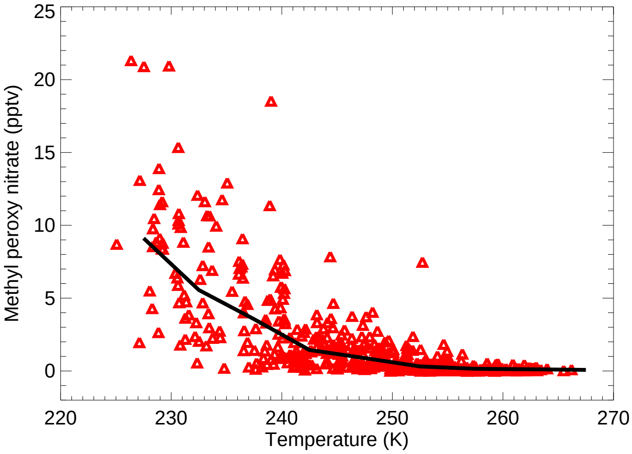

Fig. 1. Methyl peroxy nitrate concentration inferred from observations. The black line represents temperature binned median values.

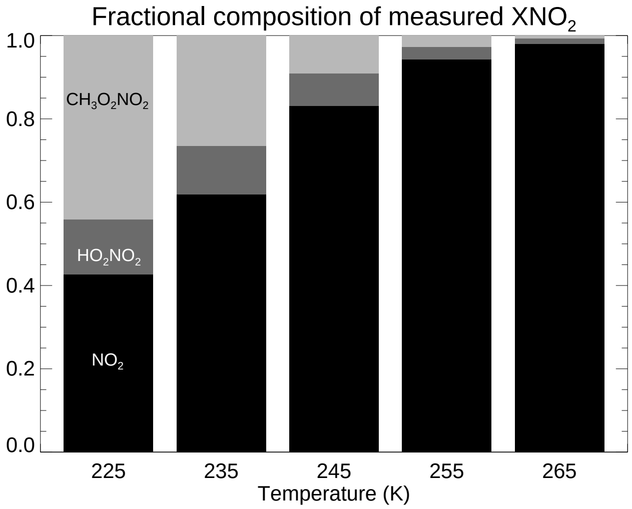

Fig. 2. Fractional composition of the XNO_2 measured by the UC Berkeley LIF nitrogen oxides instrument calculated using the photostationary state model constrained to total measured XNO_2. We estimate that 48–77 % of $CH_3O_2NO_2$ and 3–6 % of HO_2NO_2 dissociate in the inlet prior to detection.

within the uncertainty of a simpler calculation of steady state NO_2 using only the measured NO_2 photolysis rate and the NO, ozone, and HO_2 concentrations.

The residence time in the UC Berkeley LIF was determined in the laboratory after ARCTAS was completed by varying inlet and outlet pressures to simulate aircraft conditions and measuring the flows. Due to the difficulties in simulating aircraft conditions in the lab, we assign an uncertainty of ±25 % to our residence time. An increase of 25 % in the residence time leads to decreases of approximately 10 % in both NO_2 and $CH_3O_2NO_2$ concentrations at 230–235 K. A decrease in residence time of 25 % results in ~10 % increases of NO_2 and $CH_3O_2NO_2$ in the same temperature range. A decrease in residence time results in an increase in both NO_2 and $CH_3O_2NO_2$ because the decreased residence time results in smaller fractions of $CH_3O_2NO_2$ and HO_2NO_2 that dissociate in the inlet. Since we force the sum of dissociated $CH_3O_2NO_2$, dissociated HO_2NO_2, and calculated NO_2 to equal the measured XNO_2, the decrease in the fractions of $CH_3O_2NO_2$ and HO_2NO_2 that dissociate results in a larger concentration of NO_2 and thus a higher calculated steady state $CH_3O_2NO_2$.

The concentrations of $CH_3O_2NO_2$ calculated by the photostationary state model and constrained by the XNO_2 observations reach values of up to ~5–15 pptv in the coldest conditions sampled during ARCTAS (Fig. 1). It is probable that larger concentrations of $CH_3O_2NO_2$ were present during ARCTAS in conditions under which our photostationary state assumption fails. Under these conditions, the median $CH_3O_2NO_2$ mixing ratio is ~1.6 times larger than that of NO_2. As shown in Fig. 2, at temperatures below 240 K, $CH_3O_2NO_2$ ranges from ~27–43 % of XNO_2 while thermal dissociation of HO_2NO_2 contributes ~11–14 %. The resulting NO_2 shows improved agreement with NO_2 predicted from measured NO, HO_2, and NO_2 photolysis values at temperatures ~ 245 K and below (not shown). Since $CH_3O_2NO_2$ is approximately equal to NO_2 at temperatures below 240 K, it serves as an important NO_x reservoir that will release NO_x when the air mass warms, potentially doubling the NO_2 concentration. This source of CH_3O_2 and NO_2 radicals will increase ozone production and affect NO_x and HO_x chemistry. In order to investigate this more completely, we added $CH_3O_2NO_2$ chemistry to the global 3-D chemical transport model GEOS-Chem.

4 Global 3-D CTM model results

The GEOS-Chem model (version 08-02-02) was run at 2×2.5 degree resolution. The standard chemistry in the model is described in detail in Mao et al. (2010). Two separate runs were conducted: one with $CH_3O_2NO_2$ reactions added to the standard chemistry (hereinafter referred to as the methyl peroxy nitrate or MPN case) and one with only the standard chemistry (hereinafter referred to as the base case). The $CH_3O_2NO_2$ reactions consisted of Reactions (R7), (R8) and (R13) from Table 2. As in the photostationary state model, photolysis of $CH_3O_2NO_2$ was calculated assuming that the UV cross sections were equal to those of HO_2NO_2 and that IR photolysis of $CH_3O_2NO_2$ resulting from vibrational overtone excitation was negligible.

Both models were run from January–December 2007 to remove memory of the initialization. We analyze output for January–December 2008. Twenty-four hour averaged concentrations are saved for both the first and second half of each month. In this analysis we focus on the resulting changes in tropospheric concentrations to NO_x, ozone, N_2O_5, HO_2NO_2,

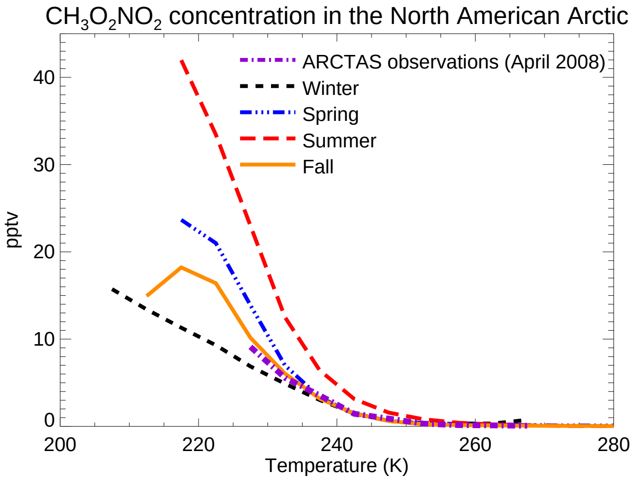

Fig. 3. Temperature binned mean values of the GEOS-Chem modeled $CH_3O_2NO_2$ 24 h average concentrations over the North American Arctic for each season.

HNO_3, and methyl hydrogen peroxide. We choose these species as examples to illustrate that due to the highly coupled, non-linear relationship between NO_x and HO_x, altering NO_x concentrations by including $CH_3O_2NO_2$ chemistry changes: the cycling of NO_x (and thus ozone concentrations), both short (N_2O_5, HO_2NO_2) and long-term (HNO_3) NO_x reservoirs and sinks, and HO_x reservoirs (CH_3OOH). We do not attempt a thorough budget analysis of the changes in all of these species; our goal is to illustrate how changes resulting from inclusion of $CH_3O_2NO_2$ chemistry affect tropospheric composition. Significant changes in tropospheric composition, particularly at cold temperatures, result when $CH_3O_2NO_2$ chemistry is included. We present seasonal mean results for the North American Arctic (defined here as 175° W–35° W and 65° N–85° N) and summertime (June, July, August) results from the tropics (defined here as 180° W–180° E and 20° S–20° N). We restrict this analysis to the troposphere by only using results in the model's vertical layers below the layer containing the tropopause.

4.1 North American Arctic

As shown in Fig. 3, the mean value for modeled $CH_3O_2NO_2$ in the coldest conditions ($\sim$220 K) during the summertime (June, July, August) in the North American Arctic is $\sim$40 pptv. During winter (December, January, February), concentrations are lower due to decreased production. The spring (March, April, May) concentrations are slightly higher than the concentrations inferred from the ARCTAS observations of XNO_2 (Sect. 3). We expect that part of this discrepancy is due to exclusion of non-photostationary state conditions from the ARCTAS observations. $CH_3O_2NO_2$ acts as a NO_x reservoir and including it in the GEOS-Chem model results in $\sim$14–23 % less NO_x ($\sim$12 pptv in the summer) (Fig. 4a) as compared to the base case. As a result, in the summer, when photochemistry is most active, ozone is reduced by 1.2 % (1.3 ppbv) (Fig. 4b). In the winter, ozone is reduced by 0.6 % (0.5 ppbv). Although NO_y concentrations remain unchanged, substantial differences in the partitioning of NO_y is observed. At the coldest temperatures N_2O_5 concentrations are reduced by $\sim$10–20 % ($\sim$0.2 pptv) (Fig. 4c) due to sequestration of NO_2 by $CH_3O_2NO_2$. At temperatures above $\sim$230–240 K, $CH_3O_2NO_2$ causes increases in N_2O_5 of up to 20 % in the fall (September, October, November) and 30 % in winter. Increases in HO_2NO_2 concentrations are also seen in the fall and winter (Fig. 4d). These increases result from an increase in chemical production of N_2O_5 and HO_2NO_2 in the MPN case relative to the base case. The increase in chemical production is due to increased NO_2 concentrations (at 240 K NO_2 is 20 % larger in the winter and 16 % larger in fall). This increase in NO_2 is presumably due to thermal dissociation of $CH_3O_2NO_2$. It should be noted that although these are large relative changes, they represent absolute changes of generally less than 1 pptv.

By sequestering NO_x, $CH_3O_2NO_2$ reduces NO concentrations resulting in a decreased conversion of HO_2 to OH. Consequently, OH concentrations are lower (not shown). These reductions in NO_x and OH by $CH_3O_2NO_2$ chemistry result in up to 4 % less HNO_3 ($\sim$6 pptv) in the winter and 5.5 % less HNO_3 ($\sim$15 pptv) in the summer (Fig. 4e). The HO_y species methyl hydrogen peroxide shows increases up to 14 % ($\sim$3 pptv) at $\sim$220 K in the summertime (Fig. 4f). Smaller increases occur at other times of the year. The changes in methyl hydrogen peroxide concentrations are due to increases in chemical production (resulting from higher HO_2 concentrations), increases in lifetime due to the lower OH concentrations, and changes in the concentrations transported into the region. At 220 K, chemical production is increased $\sim$4 % in the MPN case relative to the base case in the spring and in the summer it is increased by $\sim$10 %. The lifetime of methyl hydrogen peroxide in the MPN case relative to the base case increases by $\sim$6 % in the spring and $\sim$9 % in the summer.

4.2 Tropics

Although overall results from the tropics are similar to the results in the North American Arctic there are two distinct differences. First, temperatures in the upper troposphere of the tropics are lower than in the mid latitudes and polar regions due to the higher tropopause. Consequently, $CH_3O_2NO_2$ concentrations peak at temperatures of $\sim$215 K and decrease at lower temperatures (Fig. 5) as do the differences between the base and MPN cases (Figs. 6 and 7). The decrease occurs because of a reduction in CH_3O_2 formation due to the slower rate of $OH + CH_4$ at colder temperatures. The second important difference from the North American Arctic is the presence of large modeled spikes in $CH_3O_2NO_2$ concentrations (and the resulting large spikes in differences between

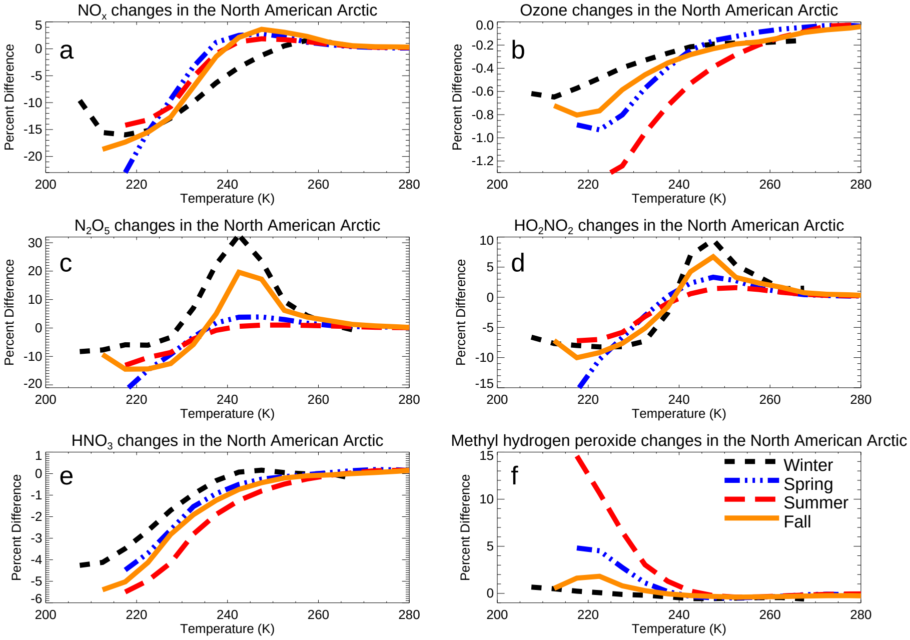

Fig. 4. Differences between the GEOS-Chem base case and MPN case (((MPN-BASE)/BASE)*100) over the North American Arctic versus temperature for **(a)** NO_x, **(b)** ozone, **(c)** N_2O_5, **(d)** HO_2NO_2, **(e)** HNO_3, and **(f)** methyl hydrogen peroxide. These results are temperature binned means of 24 h averaged concentrations.

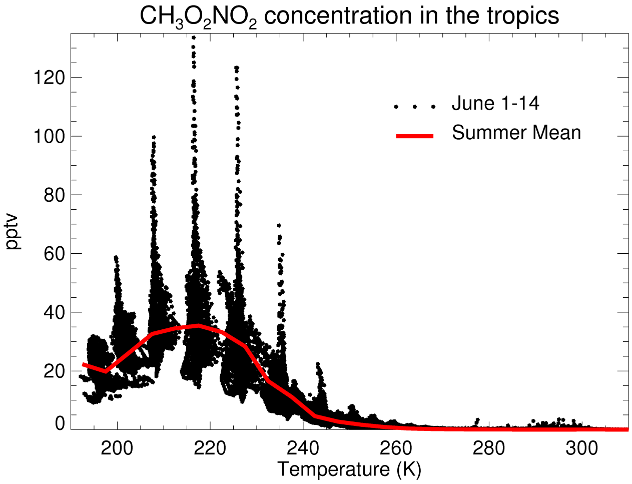

Fig. 5. Tropospheric concentrations of $CH_3O_2NO_2$ versus temperature over the tropics. The individual points are the 24 h average value of 1–14 June 2008. The red line is the summer mean concentration. The regular temperature intervals at low temperatures are a result of decreasing vertical resolution in the model at increasing altitudes.

the base and MPN cases) on the otherwise smooth curve that has the temperature dependence of $CH_3O_2NO_2$ chemistry. These spikes are due to elevated concentrations of $CH_3O_2NO_2$ downwind of biomass burning events as confirmed by large concentrations of peroxyacetyl nitrate and CO in these plumes (not shown). These spikes appear at regular intervals due to the decreased vertical resolution of the model in the upper troposphere. Each group of points are the results from a different vertical level of the model. In these particular biomass burning events, $CH_3O_2NO_2$ chemistry results in maximum changes of ∼20–40 % (25–70 pptv) less NO_x (Fig. 6a), ∼2–4 % (1.5–2.6 ppbv) less ozone (Fig. 6b), ∼20–35 % (0.7–1.2 pptv) less N_2O_5 (Fig. 6c), ∼7–20 % (1.5–6 pptv) less HO_2NO_2 (Fig. 6d), ∼7–14 % (15–40 pptv) less HNO_3 (Fig. 6e), and ∼30–75 % (20–60 pptv) more methyl hydrogen peroxide (Fig. 6f) as compared to the base case. As in the arctic, changes in methyl hydrogen peroxide are due to a combination of increased chemical production and increased lifetime in the MPN case compared to the base case. In the biomass burning plumes chemical production is up to ∼90 % faster in the MPN case and the lifetime is ∼29 % longer. Additionally, the MPN case has approximately 14–28 % less OH (Fig. 7a) and 10–25 % more HO_2 (Fig. 7b) in these plumes than in the base case.

5 Implications

Through sequestration of NO_x, $CH_3O_2NO_2$ will directly affect the NO_x budget of the upper troposphere. Since lightning emits NO_x directly into the upper troposphere, these emissions will result in proportionally more $CH_3O_2NO_2$ production than surface NO_x sources. Recently, several studies have attempted to constrain the lightning NO_x source by

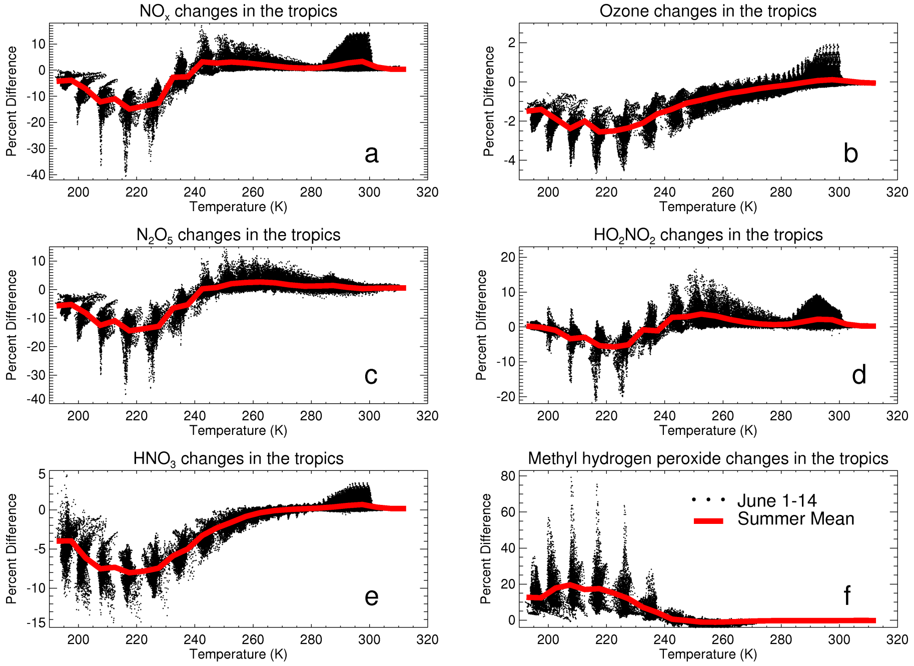

Fig. 6. Differences between the GEOS-Chem base case and MPN case (((MPN-BASE)/BASE)*100) over the tropics versus temperature for **(a)** NO_x, **(b)** ozone, **(c)** N_2O_5, **(d)** HO_2NO_2, **(e)** HNO_3, and **(f)** methyl hydrogen peroxide. The individual points are the 24 h average value of 1–14 June 2008. The red line is the summer mean concentration. The regular temperature intervals at low temperatures are a result of decreasing vertical resolution in the model at increasing altitudes.

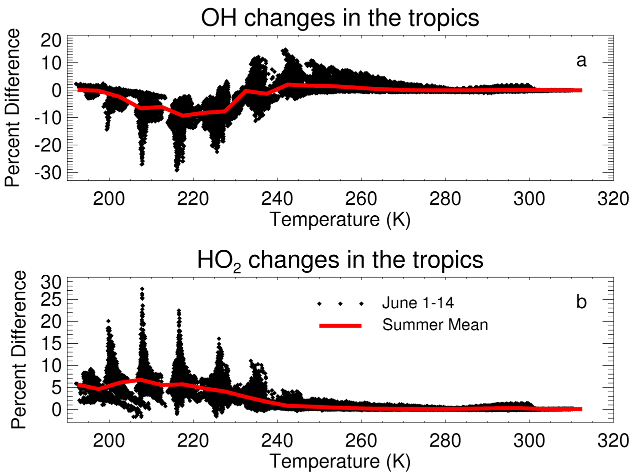

Fig. 7. Differences between the GEOS-Chem base case and MPN case (((MPN-BASE)/BASE)*100) over the tropics versus temperature for **(a)** OH and **(b)** HO_2. The individual points are the 24 h average value of 1–14 June 2008. The red line is the summer mean concentration. The regular temperature intervals at low temperatures are a result of decreasing vertical resolution in the model at increasing altitudes.

varying emissions in models and using top-down constraints from aircraft (e.g. Hudman et al., 2007) or satellite (e.g. Martin et al., 2007) measurements. It is possible that inclusion of $CH_3O_2NO_2$ chemistry will necessitate an increase in these lightning NO_x estimates; however this effect will be sensitive to the altitude of lightning NO_x emissions. Over the tropics the $CH_3O_2NO_2$ to NO_x ratio peaks at ∼30 % between 11 and 12 km altitude and then decreases to ∼15 % by ∼9.9 km and ∼14 km. Consequently, calculations of lightning NO_x emitted between 11 and 12 km will be most strongly affected by $CH_3O_2NO_2$ chemistry.

The decrease in upper tropospheric NO_x from inclusion of $CH_3O_2NO_2$ results in increases in HO_2 and decreases in OH in the upper troposphere, thus increasing the HO_2 to OH ratio. During the Intercontinental Chemical Transport Experiment-A (INTEX-A) Ren et al. (2008) found that the observed HO_2/OH ratio was larger than box-model predictions in the upper troposphere. Although the box-model used in Ren et al. (2008) contains $CH_3O_2NO_2$ chemistry, it was constrained to measured NO_2 concentrations. It is likely that these concentrations are measurements of XNO_2. We expect that the difference in the box model results constrained to XNO_2 versus the results constrained to NO_2 would be qualitatively similar to the changes observed between our base case and MPN case GEOS-Chem runs. The magnitude of the change in HO_2 between the MPN and base case runs is significantly smaller than the

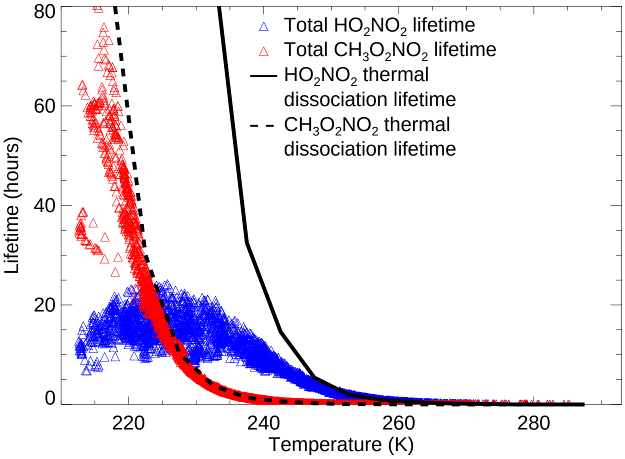

Fig. 8. Temperature dependence of $CH_3O_2NO_2$ and HO_2NO_2 lifetimes for conditions sampled during ARCTAS. Symbols represent total lifetimes and solid lines are 5 K binned thermal lifetimes. IR photolysis for HO_2NO_2 is estimated as $1\times10^{-5}\,s^{-1}$ (∼27.8 h).

measurement-model differences observed during INTEX-A by Ren et al. (2008). We conclude that $CH_3O_2NO_2$ interference in the NO_2 measurement during INTEX-NA may be responsible for part of the difference between measured and modeled HO_x and NO_x during INTEX-NA, but there are still unexplained measurement-model discrepancies.

It is also interesting to note that because both the reaction with OH and IR photolysis are negligible loss process for $CH_3O_2NO_2$, $CH_3O_2NO_2$ has a longer lifetime than HO_2NO_2 at temperatures below ∼225 K (symbols in Fig. 8) under daytime conditions. Therefore, in the coldest conditions of the upper troposphere during the day, $CH_3O_2NO_2$ is a more effective reservoir of NO_x and HO_x than HO_2NO_2. However, at night the lifetimes of $CH_3O_2NO_2$ and HO_2NO_2 will be controlled only by thermal decomposition (lines in Fig. 8) and $CH_3O_2NO_2$ will have a much shorter lifetime. For instance, assuming nine hours of darkness at 225 K, 40 % of $CH_3O_2NO_2$ will decompose, releasing CH_3O_2 and NO_2, whereas HO_2NO_2 will remain intact. Thus, these two species will have different diurnal effects on the radical concentrations.

By using reduced pressures, shorter residence times (e.g. Bradshaw et al., 1999), or some combination thereof, it is possible for future inlet designs for upper tropospheric NO_2 measurements to minimize the interference of $CH_3O_2NO_2$. In the TD-LIF system this would enable detection of $CH_3O_2NO_2$ solely in the peroxy nitrates channel. Although TD-LIF provides the sum measurement of all peroxy nitrate species, an indirect measurement of $CH_3O_2NO_2$ would be possible using the difference between the TD-LIF signal and speciated peroxy acetyl nitrates and pernitric acid measurements.

6 Conclusions

Measurements from ARCTAS indicate that the thermally unstable $CH_3O_2NO_2$ dissociates in the inlet of NO_2 instruments resulting in upper tropospheric measurements of NO_2 that are better described as thermally labile nitrogen (XNO_2). Using the measurements of XNO_2 during ARCTAS we show that in the coldest conditions sampled, $CH_3O_2NO_2$ is present at concentrations approximately equal to or greater than NO_2. Inclusion of $CH_3O_2NO_2$ chemistry in the GEOS-Chem model results in changes in concentrations of NO_x and HO_x and their reservoirs (such as N_2O_5, HNO_3, and methyl hydrogen peroxide). The magnitude of the changes vary by season and region, however our results indicate that the addition of $CH_3O_2NO_2$ chemistry to GEOS-Chem results in significant changes whenever the temperature is below 240 K. These changes affect the calculated production and loss rates of NO_x and HO_x, the upper tropospheric HO_2 to OH ratio and the spatial distribution of NO_x and HO_x reservoirs. As shown by the results from the North American Arctic, addition of $CH_3O_2NO_2$ chemistry to models results in changes to the seasonal cycles of NO_y and HO_y species, particularly in the increase in N_2O_5 and HO_2NO_2 between 230 K and 260 K. The results from the tropics also indicate that $CH_3O_2NO_2$ plays an important role in the evolution of biomass burning plumes that are lofted to high altitudes. By sequestering both CH_3O_2 and NO_2, $CH_3O_2NO_2$ changes the chemical evolution and ozone production potential of these plumes.

Acknowledgements. The analysis described here was funded by NASA grant NNX08AE56G and a NASA Earth Systems Science Fellowship to ECB. Acetone measurements were supported by the Austrian Research Promotion Agency (FFG-ALR) and the Tiroler Zukunftstiftung and carried out with the help/support of T. Mikoviny, M. Graus, A. Hansel and T. D. Maerk. We thank William H. Brune for use of the OH and HO_2 measurements, Glenn Diskin for use of the methane and water measurements, and John D. Crounse and Paul O. Wennberg for the use of California Institute of Technology CIMS data. We also thank the ground and flight crews of the DC-8 for their hard work and logistical support during ARCTAS and the ARCTAS science team for their hard work. ECB would like to thank Rynda Hudman for her help with setting up the GEOS-Chem model.

Edited by: B. N. Duncan

References

Apel, E. C, Hills, A. J., Lueb, R., Zindel, S., Eisele, S., and Riemer, D. D.: A fast-GC/MS system to measure C_2 to C_4 carbonyls and methanol aboard aircraft, J. Geophys. Res., 108, 8794, doi:10.1029/2002JD003199, 2003.

Atlas, E. L., Ridley, B. A., and Cantrell, C. A.: The Tropospheric Ozone Production about the Spring Equinox (TOPSE) Experiment: Introduction, J. Geophys. Res., 108, 8353, doi:8310.1029/2002JD003172, 2003.

Atkinson, R., Baulch, D. L., Cox, R. A., Crowley, J. N., Hampson, R. F., Hynes, R. G., Jenkin, M. E., Rossi, M. J., and Troe, J.: Evaluated kinetic and photochemical data for atmospheric chemistry: Volume I – gas phase reactions of O_x, HO_x, NO_x and SO_x species, Atmos. Chem. Phys., 4, 1461–1738, doi:10.5194/acp-4-1461-2004, 2004.

Atkinson, R., Baulch, D. L., Cox, R. A., Crowley, J. N., Hampson, R. F., Hynes, R. G., Jenkin, M. E., Rossi, M. J., Troe, J., and IUPAC Subcommittee: Evaluated kinetic and photochemical data for atmospheric chemistry: Volume II – gas phase reactions of organic species, Atmos. Chem. Phys., 6, 3625–4055, doi:10.5194/acp-6-3625-2006, 2006.

Bacak, A., Bardwell, M. W., Raventós-Duran, M. T., Percival, C. J., Hamer, P. D., and Shallcross, D. E.: Kinetics of the CH_3O_2 + NO_2 reaction: A temperature and pressure dependence study using chemical ionisation mass spectrometry, Chem. Phys. Lett., 419, 125–129, 2006.

Bertram, T. H., Cohen, R. C., Thorn, W. J., and Chu, P. M.: Consistency of ozone and nitrogen oxides standards at tropospherically relevant mixing ratios, J. Air Waste Manage., 55, 1473–1479, 2005.

Bey, I., Jacob, D. J., Yantosca, R. M., Logan, J. A., Field, B. D., Fiore, A. M., Li, Q., Liu, H. Y., Mickley, L. J., and Schultz, M. G.: Global modeling of tropospheric chemistry with assimilated meteorology: Model description and evaluation, J. Geophys. Res., 106(D19), 23073–23095, 2001.

Bradshaw, J., Davis, D., Crawford, J., Chen, G., Shetter, R., Müller, M., Gregory, G., Sachse, G., Blake, D., Heikes, B., Singh, H., Mastromarino, J., and Sandholm, S., Photofragmentation Two-Photon Laser-Induced Fluorescence Detection of NO_2 and NO: Comparison of Measurements with Model Results Based on Airborne Observations during PEM-Tropics A, Geophys. Res. Lett., 26(4), 471–474, 1999.

Cantrell, C. A., Edwards, G. D., Stephens, S., Mauldin, R. L., Sondlo, M. A., Kosciuch, D., Eisele, F. L., Shetter, R. E., Lefer, B. L., Hall, S., Flocke, F., Weinheimer, A., Fried, A., Apel, E., Kondo, Y., Blake, D. R., Blake, N. J., Simpson, I. J., Bandy, A. R., Thornton, D. C., Heikes, B. G., Singh, H. B., Brune, W. H., Harder, H., Martinez, M., Jacob, D. J., Avery, M. A., Barrick, J. D., Sachse, G. W., Olson, J. R., Crawford, J. H., and Clarke, A. D.: Peroxy radical behavior during the Transport and Chemical Evolution over the Pacific (TRACE-P) campaign as measured aboard the NASA P-3B aircraft, J. Geophys. Res., 108, 8797, doi:10.1029/2002JD002715, 2003a.

Cantrell, C. A., Mauldin, L., Zondlo, M.,Eisele, F., Kosciuch, E., Shetter, R., Lefer, B., Hall, S., Campos, T., Ridley, B., Walega, J., Fried, A., Wert, B., Flocke, F., Weinheimer, A., Hannigan, J., Coffey, M., Atlas, E., Stephens, S., Heikes, B., Snow, J., Blake, D., Blake, N., Katzenstein, A., Lopez, J., Browell, E. V., Dibb, J., Scheuer, E., Seid, G., and Talbot, R.: Steady state free radical budgets and ozone photochemistry during TOPSE, J. Geophys. Res. 108, 8361, doi:10.1029/2002JD002198, 2003b.

Cantrell, C. A.: Technical Note: Review of methods for linear least-squares fitting of data and application to atmospheric chemistry problems, Atmos. Chem. Phys., 8, 5477–5487, doi:10.5194/acp-8-5477-2008, 2008.

Cleary, P. A., Wooldridge, P. J., and Cohen, R. C.: Laser-induced fluorescence detection of atmospheric NO_2 with a commercial diode laser and a supersonic expansion, Appl. Optics, 41, 6950–6956, 2002.

Crawford, J., Davis, D., Chen, G., Bradshaw, J., Sandholm, S., Gregory, G., Sachse, G., Anderson, B., Collins, J., Blake, D., Singh, H., Heikes, B., Talbot, R., and Rodriguez, J.: Photostationary state analysis of the NO_2-NO system based on airborne observations from the western and central North Pacific, J. Geophys. Res., 101, D1, 2053–2072, 1996.

Crounse, J., McKinney, K. A., Kwan, A. J., and Wennberg, P. O.: Measurement of gas-phase hydroperoxides by chemical ionization mass spectrometry, Anal. Chem., 78, 6726–6732, 2006.

Crounse, J. D., DeCarlo, P. F., Blake, D. R., Emmons, L. K., Campos, T. L., Apel, E. C., Clarke, A. D., Weinheimer, A. J., McCabe, D. C., Yokelson, R. J., Jimenez, J. L., and Wennberg, P. O.: Biomass burning and urban air pollution over the Central Mexican Plateau, Atmos. Chem. Phys., 9, 4929–4944, doi:10.5194/acp-9-4929-2009, 2009.

Diskin, G. S., Podolske, J. R., Sachse, G. W., and Slate, T. A.: Open-Path Airborne Tunable Diode Laser Hygrometer, in: Diode Lasers and Applications in Atmospheric Sensing, edited by: Fried, A., SPIE Proceedings, 4817, 196–204, 2002.

Faloona, I. C., Tan, D., Lesher, R. L., Hazen, N. L., Frame, C. L., Simpas, J. B., Harder, H., Martinez, M., Di Carlo, P., Ren, X., and Brune, W. H.: A laser-induced fluorescence instrument for detecting tropospheric OH and HO_2: Characteristics and calibration, J. Atmos. Chem., 47, 139–167, 2004.

Golden., D. M.: Evaluating data for atmospheric models, an example: CH_3O_2 + NO_2 = $CH_3O_2NO_2$, Int. J. Chem. Kinet., 37, 10, 625–632, 2005.

Hudman, R. C., Jacob, D. J., Turquety, S., Leibensperger, E. M., Murray, L. T., Wu, S., Gilliland, A. B., Avery, M., Bertram, T. H., Brune,W., Cohen, R. C., Dibb, J. E., Flocke, F. M., Fried, A., Holloway, J., Neuman, J. A., Orville, R., Perring, A., Ren, X., Sachse, G.W., Singh, H. B., Swanson, A., and Wooldridge, P. J.: Surface and lightning sources of nitrogen oxides over the United States: Magnitudes, chemical evolution, and outflow, J. Geophys. Res., 112, D12S05, doi:10.1029/2006JD007912, 2007.

Jacob, D. J., Crawford, J. H., Maring, H., Clarke, A. D., Dibb, J. E., Emmons, L. K., Ferrare, R. A., Hostetler, C. A., Russell, P. B., Singh, H. B., Thompson, A. M., Shaw, G. E., McCauley, E., Pederson, J. R., and Fisher, J. A.: The Arctic Research of the Composition of the Troposphere from Aircraft and Satellites (ARCTAS) mission: design, execution, and first results, Atmos. Chem. Phys., 10, 5191–5212, doi:10.5194/acp-10-5191-2010, 2010.

Kim, S., Huey, L. G., Stickel, R. E., Tanner, D. J., Crawford, J. H., Olson, J. R., Chen, G., Brune, W. H., Ren, X., Lesher, R., Wooldridge, P. J., Bertram, T. H., Perring, A., Cohen, R. C., Lefer, B. L., Shetter, R. E., Avery, M., Diskin, G., and Sokolik, I.: Measurement of HO_2NO_2 in the free troposphere during the Intercontinental Chemical Transport Experiment-North America 2004, J. Geophys. Res., 112, D12S01, doi:10.1029/2006JD007676, 2007.

Mao, J., Jacob, D. J., Evans, M. J., Olson, J. R., Ren, X., Brune, W. H., Clair, J. M. St., Crounse, J. D., Spencer, K. M., Beaver, M. R., Wennberg, P. O., Cubison, M. J., Jimenez, J. L., Fried, A., Weibring, P., Walega, J. G., Hall, S. R., Weinheimer, A. J., Cohen, R. C., Chen, G., Crawford, J. H., McNaughton, C., Clarke, A. D., Jaeglé, L., Fisher, J. A., Yantosca, R. M., Le Sager, P., and Carouge, C.: Chemistry of hydrogen oxide radicals (HO_x) in the Arctic troposphere in spring, Atmos. Chem. Phys., 10, 5823–

5838, doi:10.5194/acp-10-5823-2010, 2010.

Martin, R. V., Sauvage, B., Folkins, I., Sioris, C. E., Boone, C., Bernath, P., and Ziemke, J.: Space-based constraints on the production of nitric oxide by lightning, J. Geophys. Res., 112, D09309, doi:10.1029/2006.JD007831, 2007.

Murphy, J. G., Thornton, J. A., Wooldridge, P. J., Day, D. A., Rosen, R. S., Cantrell, C., Shetter, R. E., Lefer, B., and Cohen, R. C.: Measurements of the sum of HO_2NO_2 and $CH_3O_2NO_2$ in the remote troposphere, Atmos. Chem. Phys., 4, 377–384, doi:10.5194/acp-4-377-2004, 2004.

Nizkorodov, S. A., Crounse, J. D., Fry, J. L., Roehl, C. M., and Wennberg, P. O.: Near-IR photodissociation of peroxy acetyl nitrate, Atmos. Chem. Phys., 5, 385–392, doi:10.5194/acp-5-385-2005, 2005.

Ren, X., Olson, J. R., Crawford, J. H., Brune, W. H., Mao, J., Long, R. B., Chen, Z., Chen, G., Avery, M. A., Sachse, G. W., Barrick J. D., Diskin, G. S., Huey, L. G., Fried, A., Cohen, R. C., Heikes, B., Wennberg, P. O., Singh, H. B., Blake, D. R., and Shetter, R. E.: HO_x chemistry during INTEX-A 2004: Observation, model calculation, and comparison with previous studies, J. Geophys. Res., 113, D05310, doi:10.1029/2007JD009166, 2008.

Sachse, G. W., Hill, G. F., Wade, L. O., and Perry, M. G.: Fast response, high precision carbon monoxide sensor using a tunable diode laser absorption technique, J. Geophys. Res., 92, 2071–2081, 1987.

Sander, S. P., Finlayson-Pitts, B. J., Friedl, R. R., Golden, D. M., Huie, R. E., Keller-Rudek, H., Kolb, C. E., Kurylo, M. J., Molina, M. J., Moortgat, G. K., Orkin, V. L., Ravishankara A. R., and Wine, P. H.: Chemical Kinetics and Photochemical Data for Use in Atmospheric Studies, Evaluation Number 15, JPL Publication 06-2, Jet Propulsion Laboratory, Pasadena, 2006.

Saunders, S. M., Jenkin, M. E., Derwent, R. G., and Pilling, M. J.: Protocol for the development of the Master Chemical Mechanism, MCM v3 (Part A): tropospheric degradation of non-aromatic volatile organic compounds, Atmos. Chem. Phys., 3, 161–180, doi:10.5194/acp-3-161-2003, 2003.

Shetter, R. E. and Müller, M.: Photolysis frequency measurements using actinic flux spectroradiometry during the PEM-Tropics Mission: Instrument description and some results, J. Geophys. Res., 104, 5647–5661, 1999.

Slusher, D. L., Huey, L. G., Tanner, D. J., Chen, G., Davis, D. D., Buhr, M.,Nowak, J. B., Eisele, F. L., Kosciuch, E., Mauldin, R. L., Lefer, B. L., Shetter, R. E., and Dibb, J. E.: Measurements of pernitric acid at the South Pole during ISCAT 2000, Geophys. Res. Lett., 29, 21, 2011, doi:10.1029/2002GL015703, 2002.

Slusher, D. L., Huey, L. G., Tanner, D. J., Flocke, F. M., and Roberts, J. M.: A thermal dissociation-chemical ionization mass spectrometry (TD-CIMS) technique for the simultaneous measurement of peroxyacyl nitrates and dinitrogen pentoxide, J. Geophys. Res., 109, D19315, doi:10.1029/2004JD004670, 2004.

Spencer, K. M., McCabe, D. C., Crounse, J. D., Olson, J. R., Crawford, J. H., Weinheimer, A. J., Knapp, D. J., Montzka, D. D., Cantrell, C. A., Hornbrook, R. S., Mauldin III, R. L., and Wennberg, P. O.: Inferring ozone production in an urban atmosphere using measurements of peroxynitric acid, Atmos. Chem. Phys., 9, 3697–3707, doi:10.5194/acp-9-3697-2009, 2009.

St. Clair, J. M., McCabe, D. C., Crounse, J. D., Steiner, U., and Wennberg, P. O.: Chemical ionization tandem mass spectrometer for the in situ measurement of methyl hydrogen peroxide, Rev. Sci. Instrum., 81, 094102, doi:10.1063/1.3480552, 2010.

Thompson, A. M., Singh, H. B., Stewart, R. W., Kucsera, T. L., and Kondo, Y.: A Monte Carlo study of upper tropospheric reactive nitrogen during the Pacific Exploratory Mission in the Western Pacific Ocean (PEM-West B), J. Geophys. Res., 102(D23), 28437–28446, 1997.

Thornton, J. A., Wooldridge, P. J., and Cohen, R. C.: Atmospheric NO_2: In situ laser-induced fluorescence detection at parts per trillion mixing ratios, Anal. Chem., 72, 528–539, 2000.

Vaida, V.: Spectroscopy of Photoreactive Systens: Implications for Atmospheric Chemistry, J. Phys. Chem. A, 113, 5–18, 2009.

Weinheimer, A. J., Walega, J. G., Ridley, B. A., Gary, B. L., Blake, D. R., Blake, N. J., Rowland, F. S., Sachse, G. W., Anderson, B. E., and Collins, J. E.: Meridional distributions of NO_x, NO_y, and other species in the lower stratosphere and upper troposphere during AASE II, Geophys. Res. Lett., 21, 2583–2586, 1994.

Wennberg, P. O., Salawitch, R. J., Donaldson, D. J., Hanisco, T. F., Lanzendorf, E. J., Perkins, K. K., Lloyd, S. A., Vaida, V., Gao, R. S., Hintsa, E. J., Cohen, R. C., Swartz, W. H., Kusterer, T. L., and Anderson, D. E.: Twilight observations suggest unknown sources of HO_x, Geophys. Res. Lett., 26, 1373–1376, 1999.

Wisthaler, A., Hansel, A., Dickerson, R. R., and Crutzen, P. J.: Organic trace gas measurements by PTR-MS during INDOEX 1999, J. Geophys. Res., 107, 8024, doi:10.1029/2001JD000576, 2002.

Wooldridge, P. J., Perring, A. E., Bertram, T. H., Flocke, F. M., Roberts, J. M., Singh, H. B., Huey, L. G., Thornton, J. A., Wolfe, G. M., Murphy, J. G., Fry, J. L., Rollins, A. W., LaFranchi, B. W., and Cohen, R. C.: Total Peroxy Nitrates (ΣPNs) in the atmosphere: the Thermal Dissociation-Laser Induced Fluorescence (TD-LIF) technique and comparisons to speciated PAN measurements, Atmos. Meas. Tech., 3, 593–607, doi:10.5194/amt-3-593-2010, 2010.